IAA-AAS-DyCoSS2-06-05

PERFORMANCE ANALYSIS AND EXPERIMENTAL DESIGN FOR DIFFERENTIAL OPTICAL SHADOW SENSOR

Hou Zhendong,[*] Wang Zhaokui,[†] and Zhang Yulin[‡]

The Differential Optical Shadow Sensor (DOSS) is one of the sensors to measure the displacement of proof mass in the Modular Gravitational Reference Sensor (MGRS), which is mainly used for the drag-free control loop. In this paper, the measuring principle of DOSS is presented and follows by the performance analysis for the one-dimensional measurement employing one set of DOSS. To evaluate the performance, the signals detected by the DOSS and its sensitivity are modeled mathematically with the assumption of Gaussian beams, and numerical simulation is adopted to reveal the property of the two performance parameters and the applicability of the two types of modeling presented. The experimental setup to validate the function of DOSS is designed. The work can benefit the DOSS optimization design, and offer valuable implications for the payload design applied in space mission.

INTRODUCTION

Drag-free control is to counteract the non-gravitational forces exerted on satellites by micro-thrusters or other actuators with high performance, which can provide a fairly stable platform for the construction of purely gravitational orbits.[1] Drag-free control can be applied to high precision space-borne experiments such as LISA for space gravitational wave detection[2], and the field of geodesy such as GOCE[3] and Inner-Formation Flying Satellites System[4]. As a core instrument for the implementation of drag-free control, the gravitational reference sensor (GRS) is designed to provide high precision position measurement data[5]. The GRS consists of a proof mass which can be considered to fly along a purely gravitational orbit inside the instrument, a housing shielding the proof mass from major disturbances on orbit including solar pressure and drag, and sensors set on the housing to measure the relative position between the poof mass and the housing. By employing new technologies and simple structures, the GRS is developed to the modular gravitational reference sensor (MGRS) which has two types of optical sensing technology for varied purpose[6]. To achieve science data with at least picometer precision which are required for LISA, the optical interferometer is used[7]. However, due to the limited range of the interferometer, another optical sensing method exploiting light energy is adopted to accomplish the measurement with relatively lower precision and larger range. This sensor named as optical shadow sensor may be inadequate to the science data provision for gravitational wave detection, but has the prospect of measuring with nanometer precision which is sufficient for some geodesy mission. And more

[*] Hou Zhendong, Research Center of Satellite Technology, Harbin Institute of Technology, Harbin, 150001, China.
[†] Wang Zhaokui, School of Aerospace, Tsinghua University, Beijing, 100084, China.
[‡‡] Zhang Yulin, Research Center of Satellite Technology, Harbin Institute of Technology, Harbin, 150001, China; School of Aerospace, Tsinghua University, 100084, China.

importantly, it can be used for drag-free control benefiting from its satisfying millimeter-level range.

The technology of optical shadow sensing has been applied in the Triad mission successfully, and recently Stanford University is developing the experimental system of the differential optical shadow sensor (DOSS) which is virtually a combination of two optical shadow sensors[8]. The DOSS is expected to perform better than an individual sensor by using the differential signal to eliminate the noise induced by measuring light. A CubeSat project to demonstrate the DOSS technology has been proposed at the same time, the goal of which is to arrive at a sensitivity of 1 nm at 1mHz[9].

In this paper, the measuring principle of DOSS is presented and follows by the performance analysis for the one-dimensional measurement employing one set of DOSS. To evaluate the performance, the signals detected by the DOSS and its sensitivity are modeled mathematically with the assumption of Gaussian beams, and numerical simulation is adopted to reveal the property of the two performance parameters and the applicability of the two types of modeling presented. At last, the experimental setup to validate the function of DOSS is designed.

PRINCIPLE OF DOSS AND MODEL BASIS

Principle of DOSS

The DOSS is actually the combination of two optical shadow sensors. One optical shadow sensor comprises a light emitter and a light detector. As the measured object moves between the light emitter and the light detector, it would partially block the light beam, thus the light power received by the detector would change accordingly, and the position of the object would be measured via the altered light power. Figure 1 shows the mechanism of optical shadow sensors.

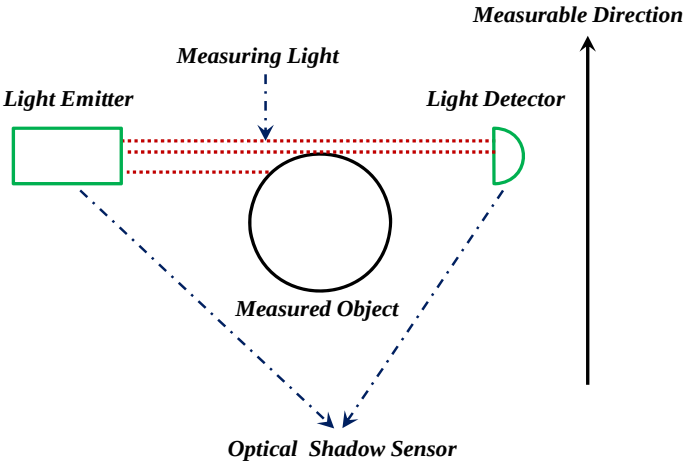

Figure 1. Illustration of the Optical Shadow Sensor

The optical shadow sensing can be understood as a measuring technique utilizing the shadow of the measured object on the detector to determine its position. Therefore, it requires the measured object to move in a specified range to guarantee the light beam is partially blocked. It is obvious that whether the light beam is completely blocked or transiting, the optical shadow sensor would be ineffective as no shadow is formed. Thus, the sensor range is limited by the size of the light spot and the photosensitive surface which determine the shadow region. If the light spot ex-

ceeds the photosensitive surface, the sensor range is restricted by the latter, and if not, the former dominates.

As the signal used by optical shadow sensor is light power, compared with the technique based on optical interference or diffraction, the coherence of light source is not demanded, and the system structure and data processing is simplified. For instance, the measured object should have a patch of clean surface to display the fringes well, and the electronics for fringe counting is essential.

In general, an optical shadow sensor can only provide the measured object's one-dimensional position data. Therefore, multiple optical shadow sensors should be combined to operate simultaneously to fulfill the three-dimensional position measurement. Furthermore, to decrease the measuring noise induced by the inaccuracy and instability of light beams, the differential signals of two optical shadow sensors can be used to accomplish the one-dimensional measuring, which is the primary trait of DOSS.

For the choice of light source, laser can be an ideal candidate due to that the high intensity and small angular spread of laser can facilitate the improvement of DOSS's sensitivity. For simplicity, the structure of the optical shadow sensor complies with the following conditions: 1) the direction of laser propagation is perpendicular to the photosensitive surface of the detector; 2) the center of the laser beam aligns with that of the photosensitive surface; 3) each laser beam has identical physical properties.

Characteristics of Gaussian Beams

The laser beam in the DOSS can be modeled as a Gaussian beam the intensity distribution of which on the transverse section can be well approximated by Gaussian functions, illustrated in Figure 2. Specifically, the intensity in the location $A(x, y, z)$ can be expressed as[10]

$$I(r,z) = I_0 \left(\frac{\omega_0}{\omega(z)} \right)^2 e^{\frac{-2r^2}{\omega^2(z)}} \tag{1}$$

where *z* axis is the direction of laser propagation, *r* is the distance from *A* to *z* axis, ω_0 is the minimum beam radius, I_0 is the maximum intensity, ω is the beam radius at the position *z*.

Assuming there is no light power attenuation during the propagation, the emitted laser power P_0 can be calculated as

$$\begin{aligned} P_0 &= I_0 \left(\frac{\omega_0}{\omega} \right)^2 \oint e^{\frac{-2r^2}{\omega^2}} dA \\ &= I_0 \left(\frac{\omega_0}{\omega} \right)^2 \int_0^{2\pi} \int_0^{\infty} e^{\frac{-2r^2}{\omega^2}} r dr d\theta \\ &= \frac{\pi}{2} I_0 \omega_0^2 \end{aligned} \tag{2}$$

ONE-DIMENSIONAL MEASUREMENT EMPLOYING THE DOSS

Providing that the proof mass is a perfect sphere with only one degree of freedom for translational motion, its position can be determined by one set of DOSS. In this section, the DOSS is placed such that the direction of motion of the proof mass is perpendicular to the direction of the laser.

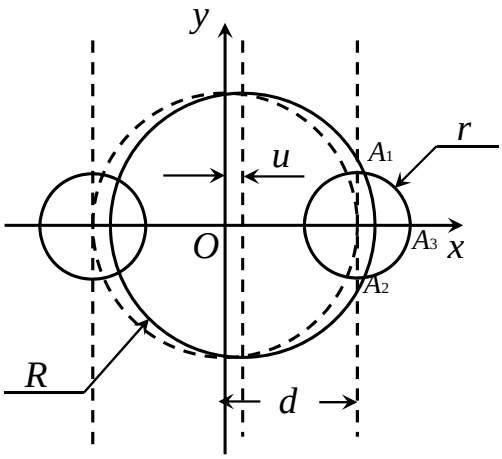

Figure 2. Illustration of the One-dimensional Measurement Using One Set of DOSS

For the convenience of modeling, a planar coordinate frame (see Figure 2) is defined with the origin on the nominal position of the geometrical center of the proof mass, the *x* axis align with the moving direction, the *y* direction orthogonal to the *x* axis, and the two axes both orthogonal to the direction of the laser beam.

Laser Power Radiated on the Detector

As shown in Figure 2, the radius of the proof mass is *R*, the photosensitive surface of the detector is circular with a radius of r, the two sensors are symmetrical with respect to the y axis, and the centers of their projection are respectively (d, 0) and (-d, 0). When the proof mass has a displacement of u, the area that can receive the laser power is changed accordingly, which is the enclosure formed by $A_1A_2A_3$ in Figure 2.

It is obvious that the curve A_1A_2 can be approximated as a line if $R \gg r$. Using the Gaussian beam property shown in Eq. (1), the laser power received by the detector in the right plane can be modeled as

$$P_+(\omega) = 2I_0\left(\frac{\omega_0}{\omega}\right)^2 \int_{R+u}^{d+r}\int_0^{\sqrt{r^2-(x-d)^2}} e^{\frac{-2\left((x-d)^2+y^2\right)}{\omega^2}} dydx \tag{3}$$

Using the relationship shown by Eq. (2), I_ω is given by

$$I_\omega = I_0\left(\frac{\omega_0}{\omega}\right)^2 = \frac{2P_0}{\pi\omega^2} \tag{4}$$

Then the laser power P_+ can be expressed as

$$P_+(\omega) = 2I_\omega \int_{R+u}^{d+r}\int_0^{\sqrt{r^2-(x-d)^2}} e^{\frac{-2\left((x-d)^2+y^2\right)}{\omega^2}} dydx \tag{5}$$

In this laser power model, the edge of the shadow is considered as a line, thus this model is named as Line Shadow Model.

However, if the condition $R \gg r$ is not satisfied, the curve A_1A_2 can't be regarded as a line. Then the Arc Shadow Model is required for analysis, which accumulates the intensity rigorously along the arc A_1A_2, and can be expressed as

$$P_+(\omega) = 2I_\omega \left[\int_{R+u}^{d+r} \int_0^{\sqrt{r^2-(x-d)^2}} e^{\frac{-2\left((x-d)^2+y^2\right)}{\omega^2}} dydx + \int_{x_c}^{R+u} \int_{\sqrt{R^2-(x-u)^2}}^{\sqrt{r^2-(x-d)^2}} e^{\frac{-2\left((x-d)^2+y^2\right)}{\omega^2}} dydx \right] \tag{6}$$

where $(x_c, y_c > 0)$ is one of the intersections formed by the contour of proof mass and that of the photosensitive surface, which is represented as

$$x_c = \frac{R^2 - r^2}{2(d-u)} + \frac{u+d}{2}, y_c = \sqrt{R^2 - (x_c - u)^2} \tag{7}$$

In the same manner, the Line Shadow Model of the laser power detected by the left sensor can be written as

$$P_-(\omega) = 2I_\omega \int_{-d-r}^{-R+u} \int_0^{\sqrt{r^2-(x+d)^2}} e^{\frac{-2\left((x+d)^2+y^2\right)}{\omega^2}} dydx \tag{8}$$

and the Arc Shadow Model can be expressed as

$$P_-(\omega) = 2I_\omega \left[\int_{-d-r}^{-R+u} \int_0^{\sqrt{r^2-(x+d)^2}} e^{\frac{-2\left((x+d)^2+y^2\right)}{\omega^2}} dydx + \int_{-R+u}^{x_c'} \int_{\sqrt{R^2-(x-u)^2}}^{\sqrt{r^2-(x+d)^2}} e^{\frac{-2\left((x+d)^2+y^2\right)}{\omega^2}} dydx \right] \tag{9}$$

where $(x_c', y_c' > 0)$ is represented as

$$x_c' = -\frac{R^2 - r^2}{2(d+u)} + \frac{u-d}{2}, y_c' = \sqrt{R^2 - (x_c' - u)^2} \tag{10}$$

Therefore, the laser power signal used for position measurement P_{diff} can be derived by differentiating the two laser powers, which is defined as

$$P_{diff} = P_- - P_+ \tag{11}$$

For the Line Shadow Model, if $d = R$, then P_- can be rewritten as

$$\begin{aligned} P_-(\omega) &= -2I_\omega \int_{R+r}^{R-u} \int_0^{\sqrt{r^2-(x-d)^2}} e^{\frac{-2\left((x-d)^2+y^2\right)}{\omega^2}} dydx \\ &= 2I_\omega \int_{R-u}^{R+r} \int_0^{\sqrt{r^2-(x'-d)^2}} e^{\frac{-2\left((x'-d)^2+y^2\right)}{\omega^2}} dydx' \end{aligned} \tag{12}$$

Combing Eq. (5), Eq. (11) and Eq. (12), the differential signal P_{diff} can be simplified as

$$\begin{aligned} P_{diff} &= 2I_\omega \left(\int_{R-u}^{R+r} \int_0^{\sqrt{r^2-(x-d)^2}} e^{\frac{-2\left((x-d)^2+y^2\right)}{\omega^2}} dydx - \int_{R+u}^{R+r} \int_0^{\sqrt{r^2-(x-d)^2}} e^{\frac{-2\left((x-d)^2+y^2\right)}{\omega^2}} dydx \right) \\ &= 2I_\omega \int_{R-u}^{R+u} \int_0^{\sqrt{r^2-(x-d)^2}} e^{\frac{-2\left((x-d)^2+y^2\right)}{\omega^2}} dydx \\ &= 4I_\omega \int_0^u \int_0^{\sqrt{r^2-x^2}} e^{\frac{-2\left(x^2+y^2\right)}{\omega^2}} dydx \end{aligned} \tag{13}$$

Adopting the Arc Shadow Model, the differential signal P_{diff} can be simplified as

$$P_{diff} = 4I_{\omega}\int_0^u \int_0^{\sqrt{r^2-x^2}} e^{\frac{-2\left(x^2+y^2\right)}{\omega^2}} dydx + \Delta P_{diff} \tag{14}$$

where

$$\begin{aligned} \Delta P_{diff} &= 2I_{\omega}\left[\int_{-R+u}^{x_c'}\int_{\sqrt{R^2-(x-u)^2}}^{\sqrt{r^2-(x+R)^2}} e^{\frac{-2\left((x+R)^2+y^2\right)}{\omega^2}} dydx - \int_{x_c}^{R+u}\int_{\sqrt{R^2-(x-u)^2}}^{\sqrt{r^2-(x-R)^2}} e^{\frac{-2\left((x-R)^2+y^2\right)}{\omega^2}} dydx\right] \\ &= 2I_{\omega}\left[\left(\int_{-x_c'-R}^{-u}\int_{\sqrt{R^2-(x+R+u)^2}}^{\sqrt{r^2-x^2}} - \int_{x_c-R}^{u}\int_{\sqrt{R^2-(x+R-u)^2}}^{\sqrt{r^2-x^2}}\right) e^{\frac{-2\left(x^2+y^2\right)}{\omega^2}} dydx\right] \end{aligned} \tag{15}$$

Model Analysis

To indicate the properties of the measurement signal based on the models established above, a simulation is carried out with the main parameters listed in Table 1, and the results are given by Figure 3.

Table 1. Parameters Used in the Simulation

r (mm)	1
ω (mm)	1.5
R (mm)	25
d (mm)	25
P_0 (mW)	1.57

It can be seen from Figure 3 that P_-, P_+ and P_{diff} vary with the change of the displacement of the proof mass approximately linearly, and the linearity is exhibited best in the central region where $u \approx 0$. While the proof mass deviates its nominal position farther, the linearity degrades. Thus, to utilize the linearity of the laser power and the displacement for measuring, the effective measurement range should be designed smaller than r.

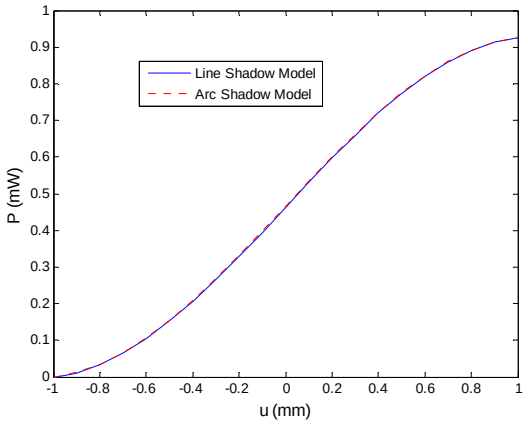

Figure 2-a) Laser Power Received by the Left Optical Shadow Sensor

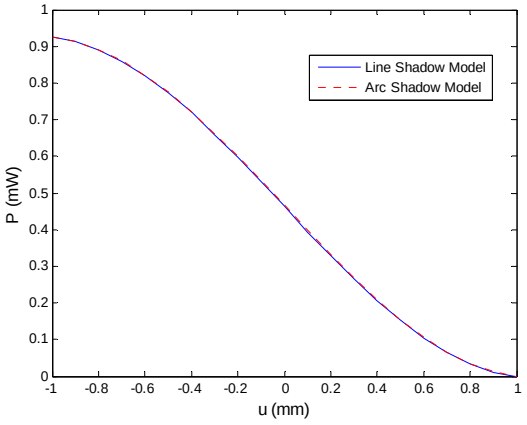

Figure 2-b) Laser Power Received by the Right Optical Shadow Sensor

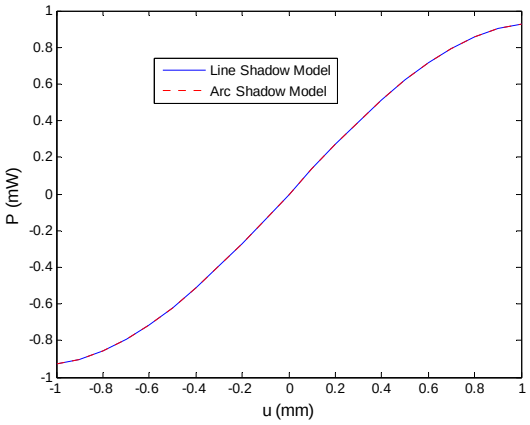

Figure 2-c) Differential Signal of DOSS

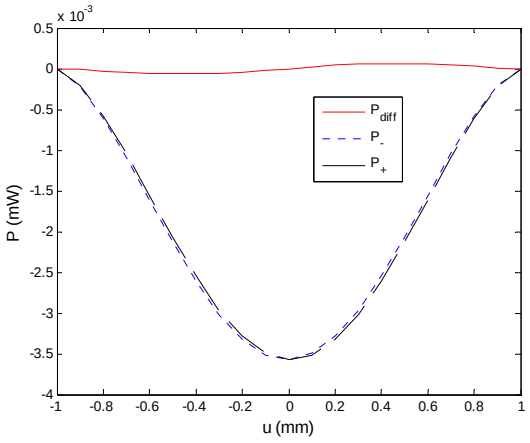

Figure 2-d) Deviation of the Signals Given by Various Models

Figure 3. Displacement-varying Laser Power Detected by Optical Shadow Sensors

The advantage of using differential laser power can also be revealed from Figure 3. It can be seen that the differential signal is almost two times sensitive to the displacement variation. For the parameters in Table 1, the variation range of the laser power received by any optical shadow sensor is about 1mW in the region from -1 mm to 1mm, whereas the differential signal can change between -1mW to 1mW approximately. The second advantage is its robustness to model error. The difference of the laser power derived by the Line Shadow Model and the Arc Shadow Model can reach $3.5\times10^{-3}\text{mW}$ at most for any optical shadow sensor, while the maximum error for the differential laser power is $\sim10^{-5}\text{mW}$. Therefore, for the measuring using differential signal, the simpler Line Shadow Model can be adopted without decreasing the model precision heavily, which is hardly applied to the situation using one sensor's signal.

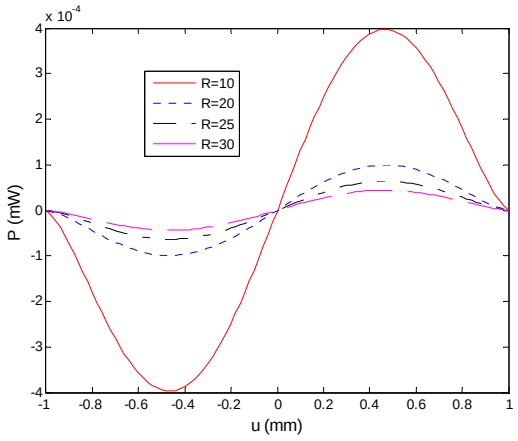

Figure 3-a) History of the Deviation of the Differential Signals Using Various Models Versus the Displacement of the Proof Mass

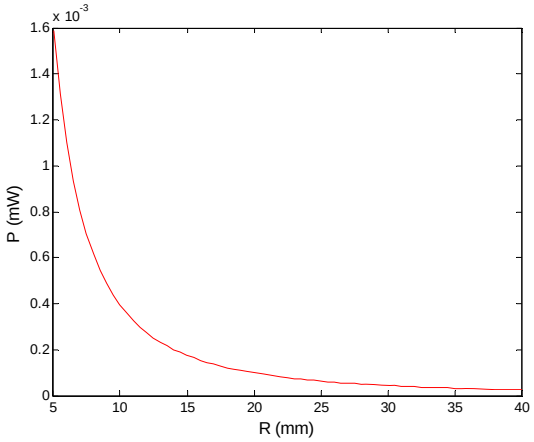

Figure 3-b) History of the Deviation of the Differential Signals Using Various Models Versus the Radius of the Proof Mass

Figure 4. Simulation Results of the Deviation of the Differential Signals Using Various Models

To illustrate more about the deviation of P_{diff} obtained by the Line Shadow Model and the Arc Shadow Model, another simulation is implemented with varied R, and the results are shown in Figure 4. It can be seen from the left figure that for various R the maximum deviation of P_{diff} occurs at approximately 0.5mm which is half the radius r, and the magnitude decreases with the increase of R. The results shown by the right figure are obtained for the parameter $u = 0.5\text{mm}$ and $R = 5 \sim 40\text{mm}$. It is obvious that the deviation of P_{diff} reduces dramatically for $R < 10\text{mm}$, whereas changes smoothly for the rest. If the deviation of P_{diff} smaller than $1\times10^{-4}\text{mW}$ can be regarded as the condition of the Line Shadow Model to be effective and reliable, R should be larger than 20mm for the parameters used here, namely the ratio of R/r should exceed 20.

Sensitivity of DOSS

Besides the output signal P_{diff}, another significant performance parameter is the sensitivity of DOSS which can defined as the varied amount of measurement signal induced by a given displacement of proof mass. The sensitivity designated as S_{DOSS} can be used to evaluate the sensor's capacity to distinguish very small position variation, and determines the sensor's measuring precision greatly which can also be influenced by the noise level.

For P_{diff} represented by Eq. (13), the sensitivity can be derived as

$$\begin{aligned} S_{DOSS} &= \frac{\partial P_{diff}}{\partial u} = \frac{\partial P_{-}}{\partial(-R+u)} - \frac{\partial P_{+}}{\partial(R+u)} \\ &= 2I_{\omega}\left[e^{\frac{-2(-R+u+d)^2}{\omega^2}} \int_0^{\sqrt{r^2-(-R+u+d)^2}} e^{\frac{-2y^2}{\omega^2}} dy + e^{\frac{-2(R+u-d)^2}{\omega^2}} \int_0^{\sqrt{r^2-(R+u-d)^2}} e^{\frac{-2y^2}{\omega^2}} dy \right] \end{aligned} \tag{16}$$

For the sensor layout that makes the range of the two laser beams equal to the diameter of the proof mass, namely $d = R$, Eq. (16) can be simplified as

$$S_{DOSS} = 4I_{\omega} e^{\frac{-2u^2}{\omega^2}} \int_0^{\sqrt{r^2-u^2}} e^{\frac{-2y^2}{\omega^2}} dy \tag{17}$$

It is evident that the DOSS's sensitivity S_{DOSS} reduces with the increasing of the displacement u, and S_{DOSS} even drops to zero when $u = r$. This property makes the measurement range with high resolution more limited because the variation of P_{diff} would decrease as the proof mass deviates from its nominal position gradually.

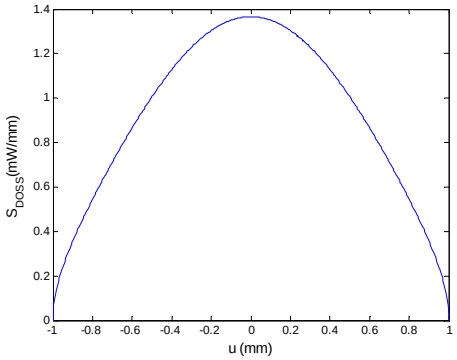

Figure 5. Sensitivity Varied with the Displacement of Proof Mass

In the condition of the parameters listed by Table 1, the sensitivity varied with the displacement is shown as Figure 5. It can be seen that if a sensitivity of 50% of the maximum number that occurs at the nominal position is required, the available range can't exceed the region between -0.7mm and 0.7mm, which is only 70% of the maximum range determined by the detector size.

EXPERIMENTAL DESIGN

To validate the performance of the DOSS, an experimental system is designed. The system is set up for one-dimensional position measurement with the precision of 1 micrometer. A solid laser is employed to generate a stable laser beam, and for the elimination of the laser noise, only one laser is used with some optical plates to form two measuring laser for the DOSS. In this way, the fluctuation of the laser power is identical for the two light beams, which means that there is little disturbance in the differential signal. As only one-dimensional measurement is required for this system, a cylinder proof mass can be used instead of a spherical one.

The function diagram for the system is presented by Figure 6. It can be seen that three types of optical plates are used. The reflectors are used to alter the laser path to accomplish the expected size and profile of the experimental system. The half-wave plates can alter the polarization state of the laser travelling through them, which can be adjusted to change the power of the two laser beams directing to the proof mass with the function of the polarizing beam splitters placed just after them. Besides the function of changing power, the polarizing beam splitters are also be used to alter the laser direction once more to make the two measuring laser propagate in parallel and orthogonal to the radial direction of the proof mass.

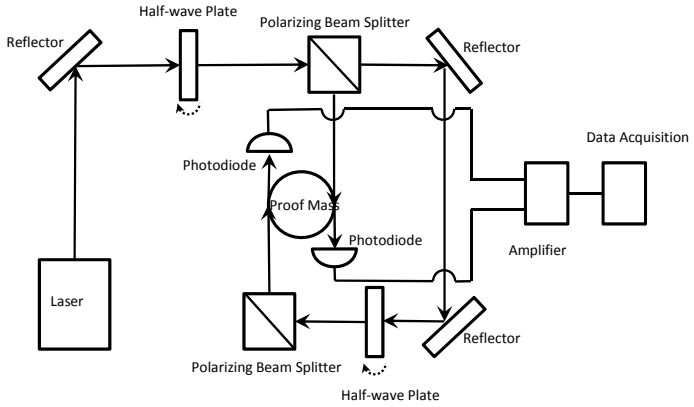

Figure 6. Function Diagram of the DOSS Experimental System

For the part of data acquisition, an amplifier and an analog-to-digital converter are required to achieve digital signals for computer processing. The amplifier uses the current induced by the laser power as input and outputs an amplified voltage signal, and the converter outputs the corresponding digital signal.

CONCLUSION

In this paper, the measured signals and sensitivity of one set of DOSS, which are critical to the sensor's performance, are mathematically modeled with the assumption of Gaussian beams. Based on numerical simulations, the measured signals derived respectively by the proposed Line Shadow Model and Arc Shadow Model are analyzed. The results reveal that the differential signal varies linearly with the displacement of proof mass in the central region, and is more robust to the model error compared to the signals on one sensor. The study of sensitivity shows that the sensitivity decreases with the increase of displacement, which sets a constraint on the measurement range. Lastly, the experimental system to validate the performance of DOSS is designed.

For the future work, the method to derive the position data via the coupled signals of multiple optical shadow sensors should be studied for three-dimensional measurement, and the optimized layout of multiple optical shadow sensors can be designed to achieve maximum performance.

REFERENCES

[1] D.B. Bebra. "Drag-free Control for Fundamental Physics Missions." *Advance in Space Research.* Vol. 32, No. 7, 2003, pp. 1221-1226.

[2] O. Jennirch. "LISA Technology and Instrumentation." *Class. Quantum Grav.* Vol. 26, No. 15, 2009, pp. 1-32.

[3] E. Canuto and A. Molano. "Drag-Free Control of the GOCE Satellite: Noise and Observer Design." *IEEE Transactions on Control Systems Technology.* Vol. 18, No. 2, 2010, pp. 501-509.

[4] Dang Z, Tang S, Xiang J, Zhang Y. "Rotational and Translational Integrated Control for Inner-formation Gravity Measurement Satellite System." *Acta Astonautica*. Vol. 75, 2012, pp. 136-153.

[5] K. Sun, G. Allen, S. Buchman, D. DeBra, R. Byer. "Advanced Gravitational Reference Sensor for High Precision Space Interferometers." *Class. Quantum Grav*. Vol. 22, No. 10, 2005, pp. 287-296.

[6] K.X. Sun, S. Buchman, R. Byer, et al. "Modular Gravitational Reference Sensor Development." *7th International LISA Symposium*, Stanford University, California, USA, 2009.

[7] J. W. Conklin, G. Allen, K.X. Sun, et al. "Determination of Spherical Test Mass Kinematics with Modular Gravitational Reference Sensor." *Journal of Guidance, Control, and Dynamics.* Vol. 31, No. 6, 2008, pp. 1700-1707.

[8] A. Zoellner, E. Hultgren, K.X. Sun. "Integrated Differential Optical Shadow Sensor for Modular Gravitational Reference Sensor." *8th International LISA Symposium*, Stanford University, California, USA, 2013.

[9] A. Zoellner, S. Buchman, J. W. Conklin, et al. "Differential Optical Shadow Sensor CubeSat Mission." *26th Annual AIAA/USU. Conference on Small Satellites.* , Utah State University, Utah, USA, 2012.

[10] W. T. Silfvast. Laser Fundamentals. Cambridge University Press, Cambridge, 2004.